Report

Cell Reports

Structural Insights into the Tumor-Promoting Function of the MTDH-SND1 Complex

Graphical Abstract

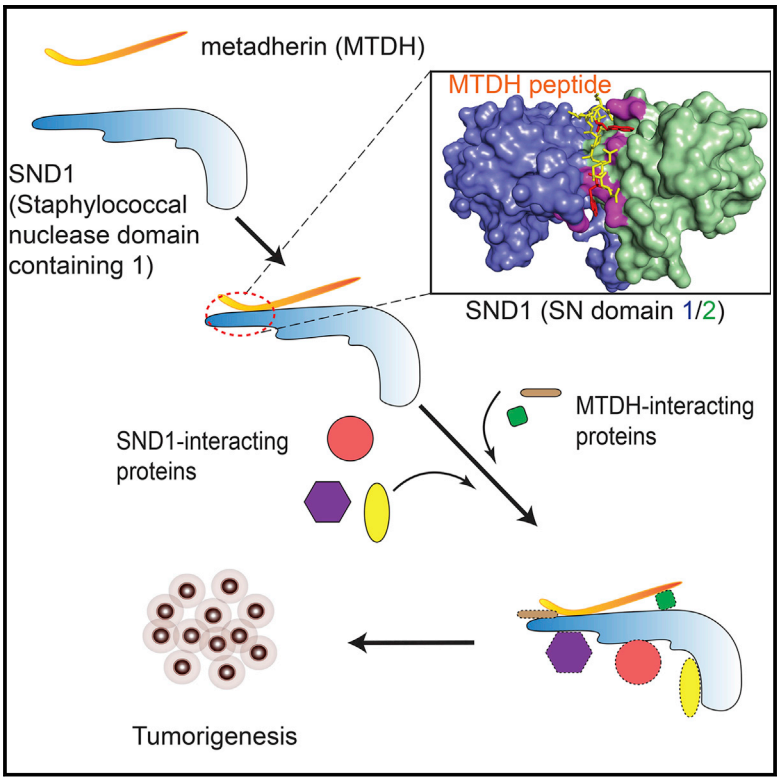

Highlights

Two tryptophan residues in MTDH bind to separate hydrophobic pockets in SND1

The MTDH-binding pockets are unique, absent in SN3/4 or other OB-fold proteins

Mutations at the MTDH-SND1 interface impair tumor initiation of breast cancer

Hydrophobic pockets in SND1 are specific targets for developing cancer therapeutics

Authors

Feng Guo, Liling Wan, ..., Yibin Kang, Yongna Xing

Correspondence

ykang@princeton.edu (Y.K.),
xing@oncology.wisc.edu (Y.X.)

In Brief

Staphylococcal nuclease domain containing 1 (SND1) was recently identified as a binding partner of Metadherin (MTDH) in multiple types of cancer. Guo et al. now determine the crystal structure of the MTDH-SND1 complex, showing the structural basis of an interaction that is essential for the tumor-promoting function. The study may facilitate the development of therapeutic strategies that target the MTDH-SND1 complex.

Accession Numbers

4QMG

Guo et al., 2014, Cell Reports 8, 1704–1713
September 25, 2014 ©2014 The Authors
http://dx.doi.org/10.1016/j.celrep.2014.08.033

OPEN ACCESS
CellPress

Cell Reports
Report

Structural Insights into the Tumor-Promoting Function of the MTDH-SND1 Complex

Feng Guo,[1,3,5] Liling Wan,[2,3] Aiping Zheng,[1] Vitali Stanevich,[1] Yong Wei,[2] Kenneth A. Satyshur,[1] Minhong Shen,[2] Woojong Lee,[1] Yibin Kang,[2,4,*] and Yongna Xing[1,4,*]

[1]McArdle Laboratory for Cancer Research, Department of Oncology, University of Wisconsin-Madison, School of Medicine and Public Health, Madison, WI 53706, USA

[2]Department of Molecular Biology, Princeton University, Princeton, NJ 08544, USA

[3]Co-first author

[4]Co-senior author

[5]Present address: Stanford University, School of Medicine, Stanford, CA 94305, USA

*Correspondence: ykang@princeton.edu (Y.K.), xing@oncology.wisc.edu (Y.X.)

http://dx.doi.org/10.1016/j.celrep.2014.08.033

SUMMARY

Metadherin (MTDH) and *Staphylococcal* nuclease domain containing 1 (SND1) are overexpressed and interact in diverse cancer types. The structural mechanism of their interaction remains unclear. Here, we determined the high-resolution crystal structure of MTDH-SND1 complex, which reveals an 11-residue MTDH peptide motif occupying an extended protein groove between two SN domains (SN1/2), with two MTDH tryptophan residues nestled into two well-defined pockets in SND1. At the opposite side of the MTDH-SND1 binding interface, SND1 possesses long protruding arms and deep surface valleys that are prone to binding with other partners. Despite the simple binding mode, interactions at both tryptophan-binding pockets are important for MTDH and SND1's roles in breast cancer and for SND1 stability under stress. Our study reveals a unique mode of interaction with SN domains that dictates cancer-promoting activity and provides a structural basis for mechanistic understanding of MTDH-SND1-mediated signaling and for exploring therapeutic targeting of this complex.

INTRODUCTION

MTDH, also known as metadherin, is overexpressed in a large spectrum of cancer types, and its elevated levels are associated with poor prognosis in cancer patients (Sarkar and Fisher, 2013; Wan and Kang, 2013). Functionally, MTDH has been implicated in several cancer-related processes, including proliferation, cell death, invasion, and angiogenesis, and has been linked to multiple oncogenic pathways such as PI3K/AKT, Wnt/β-catenin, and NF-κB (Emdad et al., 2013; Wan and Kang, 2013). However, the mechanism by which MTDH regulates these oncogenic signaling remains elusive. MTDH was originally identified as an HIV-induced gene in astrocytes, a membrane protein mediating the homing of tumor cells to the lung endothelium, and a lysine-rich protein associated with tight junctions in prostate epithelial cells (Lee et al., 2013). No functional domain has been identified in the MTDH sequence, and it interacts via its unstructured regions with diverse partners, including PLZF (Thirkettle et al., 2009), NF-κB (Sarkar et al., 2008), BCCIPα (Ash et al., 2008), and SND1 (Blanco et al., 2011; Meng et al., 2012; Yoo et al., 2011). Of note, SND1 possesses tumor-promoting function similar to that of MTDH (Blanco et al., 2011; Meng et al., 2012; Wang et al., 2012; Yoo et al., 2011).

Recently, we showed that biochemically identified MTDH mutants with compromised SND1-binding ability exhibit a reduced capacity to promote expansion and survival of tumor-initiating cells in diverse subtypes of breast cancer (Wan et al., 2014). Until now, there has been no understanding of the structure of MTDH and its binding partners, or how their structures might affect their interactions and the role of those interactions in cancer.

SND1 is a multifunctional protein harboring four tandem repeats of *Staphylococcal* nuclease (SN)-like domains at the N terminus (SN1-4), and a fusion tudor and SN domain (TSN5 domain) at the C terminus (Callebaut and Mornon, 1997; Ponting, 1997). It belongs to the oligonucleotide/oligosaccharide binding fold (OB fold) superfamily consisting of proteins that participate in DNA/RNA binding via the typical β-barrel of the OB fold (Theobald et al., 2003). SND1 has been frequently proposed as an essential component of the RNA-induced silencing complex (RISC) with involvement in miRNA-mediated silencing (Caudy et al., 2003). It was also shown to have a nuclease activity against hyperedited miRNA primary transcripts (Scadden, 2005). Structural and biochemical analysis of SND1 suggested that the N-terminal SN domains, particularly SN3/4, possess RNA binding and nuclease activity (Li et al., 2008), and the C-terminal TSN5 domain interacts with methylated Lys/Arg ligands and small nuclear ribonucleoprotein (snRNP) complexes (Shaw et al., 2007).

SND1 is among the very few members of the OB-fold superfamily that participate in interaction with diverse proteins. It was initially identified as a cellular component that enhances the transcription of EBNA-2-activated gene (Tong et al., 1995)

and later shown to interact with and modulate a broad spectrum of proteins involved in transcription (Leverson et al., 1998; Paukku et al., 2003; Välineva et al., 2005, 2006; Yang et al., 2002), including oncogenic transcription factors STAT5, STAT6, and c-Myb. In recent years, SND1 was identified as a binding partner of MTDH in multiple types of cancer and has been shown to be important for cancer cell survival under oncogenic or chemotherapeutic stresses (Blanco et al., 2011; Meng et al., 2012; Wan et al., 2014; Yoo et al., 2011). Whether the function of SND1 in cancer relies on MTDH binding remains unclear. The range of identified SND1-interacting proteins suggests that its SN domains have evolved into protein-protein interaction domains; the mode of interaction, however, remains obscure.

Because both MTDH and SND1 interact with diverse cellular machineries and signaling proteins and are implicated in multiple cancer-related cellular processes and signaling pathways, it is likely that MTDH and SND1 enhance malignant features by coordinating tumor-promoting activities via their multiple interaction domains/motifs. The complete lack of structural information, however, greatly hinders mechanistic understanding of the function of the MTDH/SND1 complex, despite the significant clinical relevance of both proteins in many types of cancer. Elucidating the structural basis of MTDH-SND1 interaction is also crucial for developing new ways of targeting MTDH or SND1 as a cancer therapeutic strategy. Here, we determined the high-resolution crystal structure of the MTDH-SND1 complex and revealed a unique interface of MTDH-SND1 interaction that is essential for the tumor-promoting function of this complex.

RESULTS

Mapping of the Minimal Regions of MTDH and SND1 Is Required for Their Interaction

The primary sequence analysis of MTDH (residues 1–582) suggested that MTDH is largely unstructured in its entire sequence except a *trans*-membrane domain near the N terminus (Figure S1). Thus, MTDH might function as a scaffold protein and recruit diverse signaling molecules via peptide motifs throughout its sequence (Figure 1A). Building on our previous observation that a MTDH fragment (364–470) harbors the essential region required for interaction with SND1 (Blanco et al., 2011), we recently mapped a minimal fragment of MTDH (386–407) within this region that confers SND1 binding similar to longer fragments of MTDH (Wan et al., 2014). None of the SND1 domains had been mapped for specific interaction with protein molecules. To address this gap, we made a handful of SND1 constructs, and two gave highly soluble recombinant proteins that harbor the N-terminal SN1/2 and the C-terminal SN3/4-TSN5 domains of SND1, respectively (Figure 1A). Using a pull-down assay with a GST-tagged MTDH (364–582), we showed that the SN1/2 domains (16–339) of SND1 bind stoichiometrically with MTDH, whereas the SN3/4-TSN5 domains (340–885) had little interaction with MTDH (Figure 1B). Further analysis of this interaction using biolayer interferometry showed that this interaction was readily reversible (Figure S2A). The binding affinity between MTDH and SND1 was determined to be around 0.6 μM by isothermal titration calorimetry (Figure S2B).

Overall Structure of the MTDH-SND1 Complex

After extensive effort, cocrystallization of the SND1 SN1/2 domains and synthetic peptides harboring MTDH residues 386–407 failed to yield protein crystals, likely due to the relatively weak interaction between the two proteins. To stabilize the complex and facilitate crystallization, we fused the SND1 SN1/2 domains to MTDH (386–407) via a flexible linker of different lengths. A variant with a 21-residue linker (STGNASDSSSDSSSSEGDGTV) yielded diffracting crystals. Although the SN1/2 domains are closely related to the SN3/4 domains, structural determination by molecular replacement using the structure of SN3/4 (Protein Data Bank [PDB] code: 3BDL) was not successful, likely due to large diversity of the extended loops emanating from the OB fold. Finally, the structure was determined by selenium SAD (single-wavelength anomalous dispersion) phasing and refined to 2.7 Å (Table S1).

Five copies of the MTDH-SND1 fusion proteins were found in each asymmetric unit that is almost identical (Figure S3A), with the root-mean-square deviation no more than 0.9 Å over 290 residues. The number of MTDH residues with defined electron density varied slightly in different copies. Nonetheless, residues 393–403 of MTDH were visible in all copies (Figure S3B). Both SN1 and SN2 exhibit the typical OB fold of *Staphylococcal* nuclease (SNase) and were arranged in a central symmetry-related fashion (Figure 1C), similar to SN3/4 (Figure 1D). Each SN domain contains a β-barrel (β1-β2-β3-β7-β5) capped by a three helix bundle (α1-α2-α3) and a short β-hairpin (β4-β8) (Figure 1C). The MTDH peptide (D_{393}WNAPAEEWGN$_{403}$) occupies the shallow groove between SN1 and SN2 domains, with the two tryptophan residues, W394 and W401, making extensive hydrophobic contacts with two well-defined hydrophobic pockets in SND1.

At the opposite side of the MTDH-SND1 interface, SND1 possesses three extended protruding structural elements (the β6-β7 hairpin in SN1 and the extended $L_{β4-α1}$ loop in both SN1 and SN2), resulting in a spiky surface capable of diverse binding modes (Figure 1C, right panel). Potential molecules with the likelihood of binding to this surface include small RNAs, components of RISC complex, or transcription factors such as STAT5, STAT6, and c-Myb that have been previously shown to interact with SND1 (Leverson et al., 1998; Li et al., 2008; Paukku et al., 2003; Välineva et al., 2005, 2006; Yang et al., 2002). The SN1/2 domains were previously suggested to participate in DNA/RNA binding (Li et al., 2008). How the hilly surface contributes to SND1 function and signaling remains to be determined.

Structural Comparison of SN1/2 with SN3/4 and SNase

Superimposition of the structures of SN1/2, SN3/4 (PDB code: 3BDL), and two copies of SNase (PDB code: 2ENB) reveals similar structures in β sheets and α helices (Figure 1D), with the root-mean-square deviation of 2.02, 1.67, and 1.68 Å over 268, 123, and 116 residues between SN1/2 and SN3/4, between SN1 and SNase, and between SN2 and SNase, respectively. Several loop regions are distinctly different, with varied length and amino acid sequences (Figures 1D and S4). As shown in detail later, the elongated $L_{β2-β3}$ loop in SN1 is crucial for mediating MTDH binding. The $L_{β4-α1}$ loops in SN1 and SN3 are significantly longer than those in SNase and adopt different

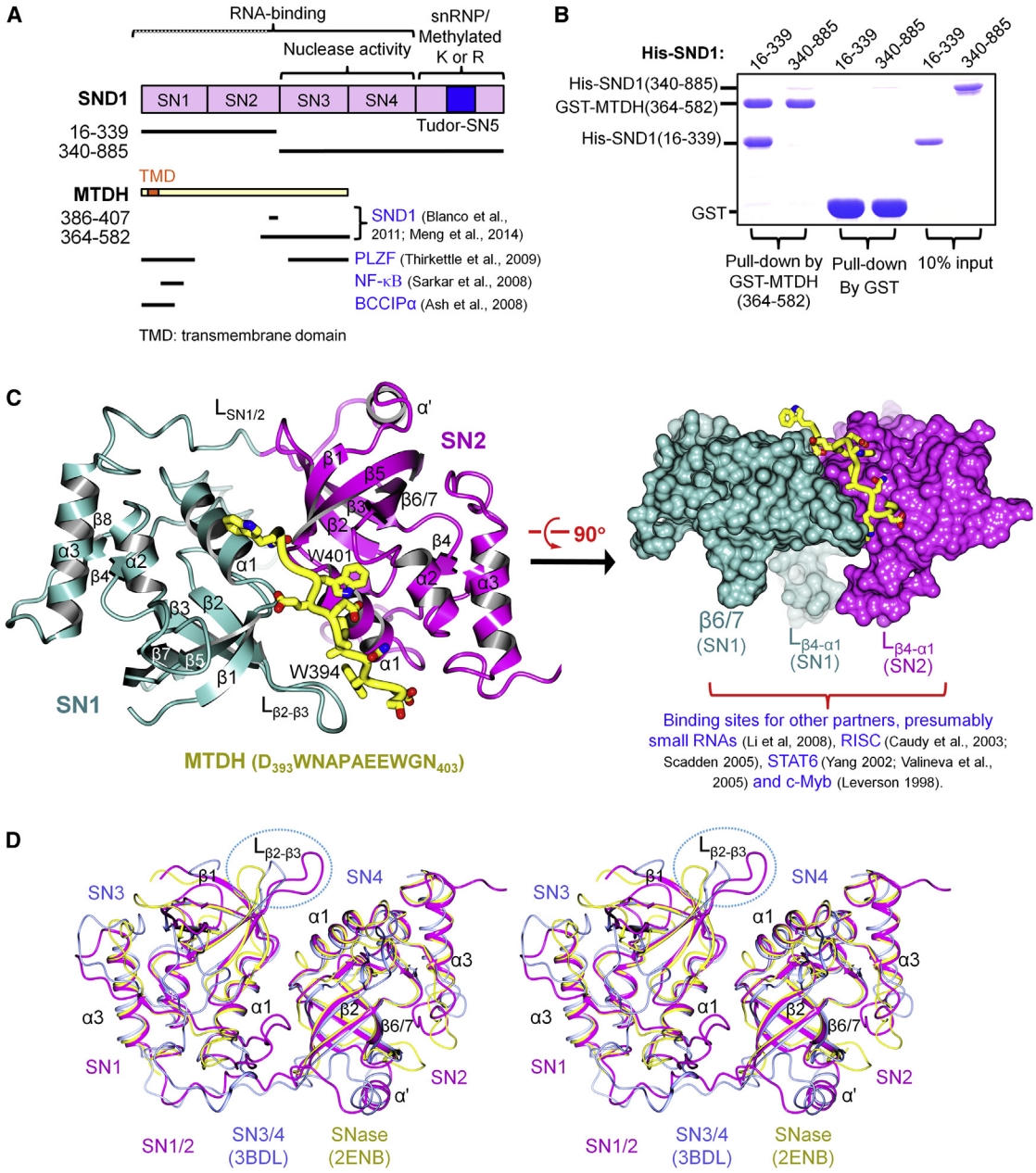

Figure 1. Mapping of SND1-MTDH Interaction and Overall Structure of Their Complex

(A) Illustration of SND1 and MTDH domain structure and motifs with known interaction partners. Soluble SND1 fragments used for studying MTDH binding and interaction motifs in MTDH are shown below.

(B) Pull-down of SND1 fragments by GST-tagged MTDH (364–582), a fragment recently shown to bind to SND1. Experiments were repeated three times; representative results are shown.

(C) Overall structure of MTDH-SND1 complex. Two perpendicular views are shown. The SN1 and SN2 domains of SND1 are colored cyan and magenta, respectively, and MTDH are colored yellow. SND1 is shown in ribbon (left) and surface (right). MTDH is shown in worm (backbone) and cylinder (side chain). See also Figures S1–S4.

(D) Overlay of the structures of SN1/2 (magenta, in the complex with MTDH), SN3/4 (blue, PDB code: 3BDL), and two models of SNase (yellow, PDB code: 2ENB) in stereo view. The difference in $L_{β2-β3}$ loop is emphasized by a dashed circle. See also Figures S1–S4.

conformations, likely defining different functionalities. Although two out of six residues at the SNase active site are retained in SN3, only one remains the same or similar in SN1 and SN4, and none is retained in SN2 (Figure S4). This is consistent with the previous observation that SN3/4 exhibits low nuclease activity, whereas SN1/2 augments nuclease activity (Li et al., 2008),

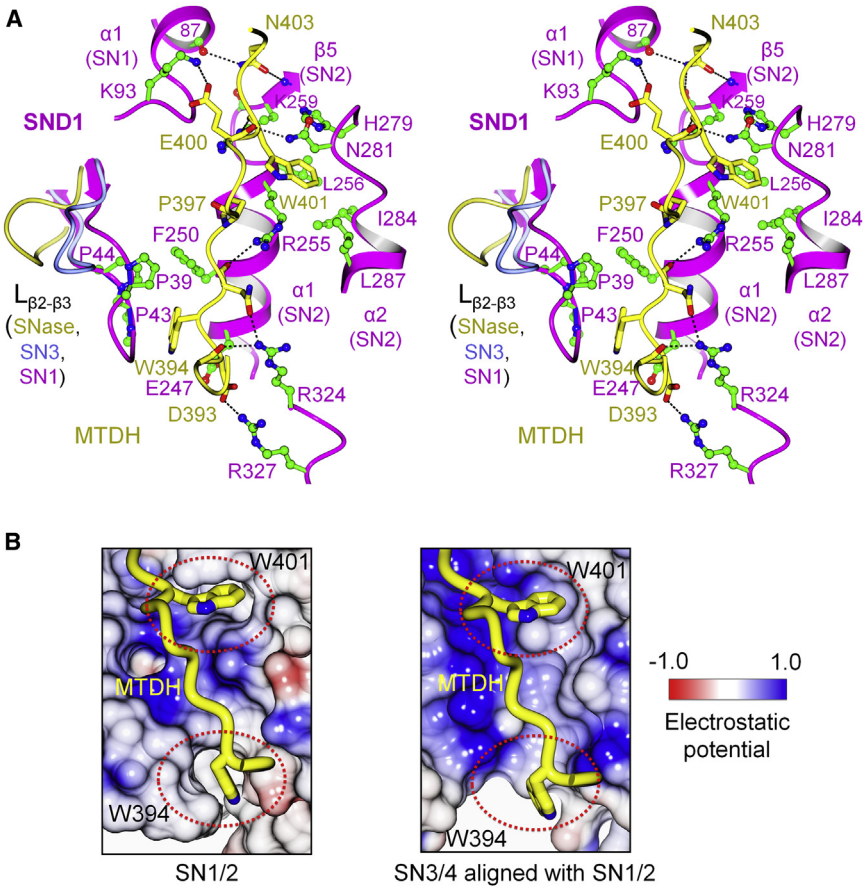

Figure 2. MTDH-SND1 Binding Interface

(A) A close-up stereo view of MTDH-SND1 interface. The structure is shown similar to Figure 1A with the same color scheme, except that the side chain of SND1 is shown in ball and stick and colored green. The $L_{\beta2\text{-}\beta3}$ loops from SN3 domain (light blue) and SNase (yellow) are shown for highlighting the unique structure of SN1 $L_{\beta2\text{-}\beta3}$ loop required for MTDH binding.

(B) A close-up view of SN1/2 electrostatic potential showing the hydrophobic pockets for binding W394 and W401 of MTDH (left). MTDH is shown in worm (backbone) and cylinder (side chain) and colored yellow. The electrostatic potential of SN3/4 reveals the absence of W394- and W401-binding pockets and the positively charged surface unfavorable for binding (right).

likely by enhancing substrate binding. These observations suggest that novel functions have evolved for the SN domains in SND1, whereas the nuclease activity in these SN folds was reduced (in SN3/4) or diminished (in SN1/2) during evolution.

MTDH-SND1 Interaction Interface

The fact that MTDH occupies an extended groove between SN1 and SN2 on the back of the hilly surface of SND1 supports the notion that MTDH might serve as a scaffold signaling protein. This architecture may allow MTDH to bridge SND1 and other MTDH-associated signaling complexes without interfering with major binding surfaces of SND1. The MTDH-SND1 interface thus provides an important basis for understanding diverse downstream signaling and their function in cancer.

The interface is dominated by hydrophobic van der Waals contacts of W394 and W401 in MTDH with two separate, well-defined hydrophobic pockets in SND1, which are buttressed by hydrogen bond (H-bond) and salt-bridge interactions at the periphery (Figure 2A). The hydrophobic pocket for W394 is formed by residues P39, P43, and P44 in the SN1 $L_{\beta2\text{-}\beta3}$ loop and the side chains of E247 and F250 on the SN2 α1 helix. The pocket for W401 is about 15 Å away and located between the α1 and α2 helices from SN2, and contoured by hydrophobic residues L256, H279, I284, and L287 and the carbon chain regions of residues R255, R259, and N281. At the periphery of the hydrophobic pockets near one end of the interface, R327 and R324 in SND1 form several H-bond and salt-bridge interactions with D393 and N395 in MTDH and its backbone carbonyl group at 392 in two of the five complexes in the asymmetric unit. In the middle, R255 in SND1 forms an H-bond interaction with the MTDH backbone at 395, and, at the other end, a few H-bond and salt-bridge interactions are formed by residues and backbone atoms from SN1 α1 helix and SN2 β5 strand with MTDH residues, E400 and N403.

The interface for MTDH binding in SND1 is highly unique and present only in SN1/2 (Figure 2B). The well-defined hydrophobic pockets for W394 and W401 are clearly shown by the surface contour of SN1/2 with electrostatic potential, but are absent in SN3/4. The surface between the two hydrophobic pockets in SN1/2 is basic, which, in part, favors the electrostatic interaction with E400, but is not ideal for interaction with nonpolar residues ($A_{396}PA_{398}$) between W394 and W401. This likely explains the relatively weak interaction between SND1 and MTDH and the fast off-rate of this interaction (Figure S2). Unlike SN1/2, the protein groove between SN3 and SN4 is largely basic, underlying another structural feature of SN3/4 that disfavors MTDH binding. Furthermore, the proline residues in the SN1 $L_{\beta2\text{-}\beta3}$ loop lining the pocket for W394 are all absent in SN3 or SNase (Figures 1D and S4), further defining the binding specificity of SN1/2 for MTDH.

Identification of MTDH and SND1 Mutants Deficient in Binding

To gain insight into how the interface characterized above contributes to MTDH-SND1 interaction, we next performed structure-guided mutagenesis studies. The structure suggests that the van der Waals hydrophobic contacts made by MTDH W394 and W401 might play a dominant role in SND1 binding. Consistent with this notion, mutating either of the two tryptophan residues to a much smaller residue alanine (W394A, W401A) or a negatively charged residue aspartate (W394D, W401D) abolished or significantly reduced the interaction between SND1

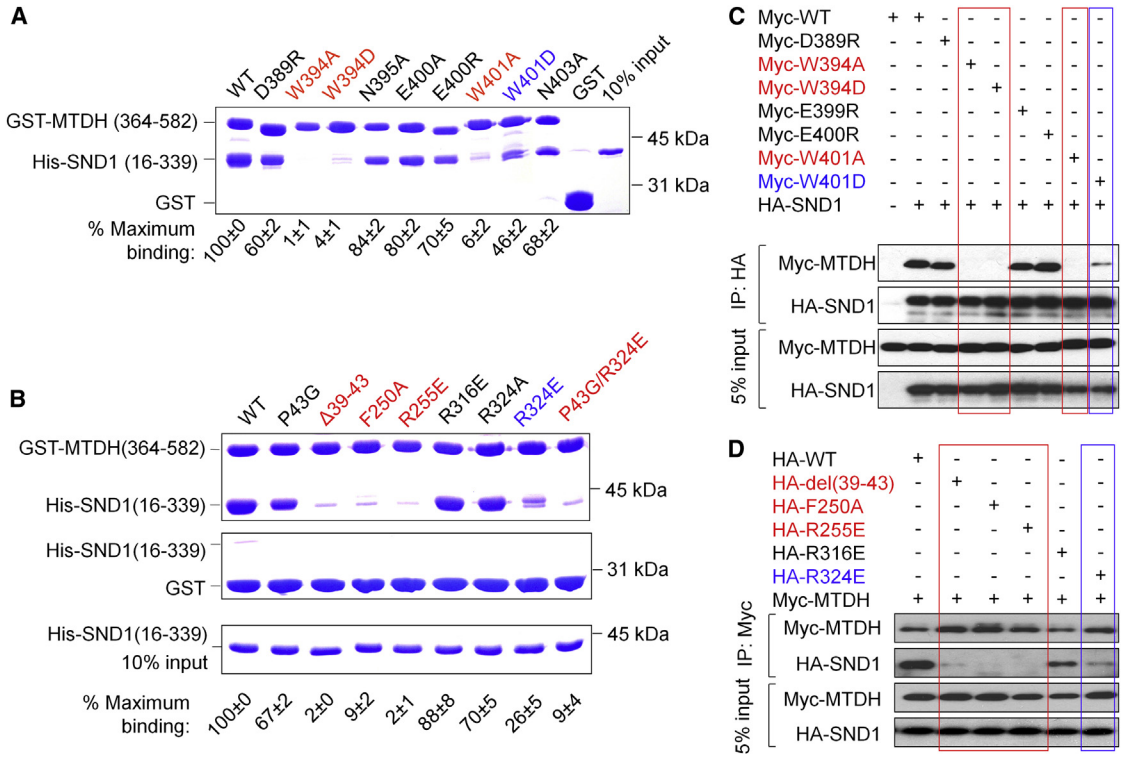

Figure 3. Identification of MTDH and SND1 Mutants Deficient in Binding

(A) In vitro pull-down of SND1 (16–339) by GST-tagged MTDH (364–582) harboring WT or mutant sequence. The proteins bound to GS4B were examined on SDS-PAGE and visualized by Coomassie blue staining.

(B) In vitro pull-down of WT and mutant SND1 (16–339) by GST-tagged MTDH (364–582). The bound proteins were examined as in (A). For both (A) and (B), experiments were repeated three times; representative results are shown. The normalized percentage of binding was averaged from three experiments; mean ± SEM was shown below the data.

(C) HEK293T cells were transfected with human HA-SND1, WT Myc-MTDH, or Myc-MTDH with indicated single point mutation. Lysates were immunoprecipitated with anti-HA antibody and immunoblotted with the indicated antibodies.

(D) HEK293T cells were transfected with human Myc-MTDH, WT HA-SND1, or mutant HA-SND1 with indicated single point mutations or deletions. Lysates were immunoprecipitated with anti-Myc and immunoblotted with the indicated antibodies.

(16–339) and MTDH (364–582) in vitro (Figure 3A). The W → A mutants exhibited stronger defects than the W → D mutants, suggesting that the MTDH-SND1 interaction is largely dictated by van der Waals contacts. The more severe defects of W394A compared to W401A likely reflect the different flexibility of the two SND1 pockets. Residues lining the pocket for W401 could adopt multiple rotamer conformations, which might partially compensate the W401A mutation for interaction with this pocket. In contrast, the binding pocket for W394 is largely conferred by three rigid proline residues and thus could barely compensate the W394A mutation. The MTDH mutations at the periphery interface (N395A, E400A, E400R, N403A), which are expected to disrupt H-bond or salt-bridge interactions, had very little effect, similar to the mutation outside the interface (D389R) (Figure 3A). These results showed that individual H-bonds make minor contributions to the MTDH-SND1 interaction and van der Waals contacts play a dominant role in this interaction.

Several SND1 mutations at the interface that disrupt MTDH binding were also identified. Changes made to the SND1 hydrophobic pockets, including R255E, F250A, and deletion in the SN1 $L_{\beta2\text{-}\beta3}$ loop (Δ39-43), almost completely abolished MTDH binding (Figure 3B). In addition to perturbing the van der Waals contacts with W401, R255E might also affect its H-bond interaction with the MTDH backbone (Figure 2A). The effect of Δ39-43 further supports the role of these residues for MTDH binding, which are unique to the SN1 $L_{\beta2\text{-}\beta3}$ loop (Figures 2 and 3B). The R324E mutation significantly weakened the MTDH binding, likely by introducing a repulsive charge-charge contact with D393 in MTDH. A different mutation to this residue, R324A, barely affected MTDH binding, similar to the mutation outside the interface, R316E.

We further examined how the MTDH and SND1 mutations identified at this interface affected the interaction of full-length proteins in mammalian cells. Full-length HA-tagged SND1 was coexpressed with full-length Myc-tagged wild-type (WT) or mutant MTDH in HEK293T cells and cell lysates were subjected to anti-HA immunoprecipitation for SND1 pull down. Consistent with in vitro observations (Figure 3A), WT MTDH, but not mutants W394A, W394D, or W401A, was pulled down along with HA-SND1 (Figure 3C, in red). MTDH mutation W401D significantly reduced the binding (Figure 3C, in blue), whereas other

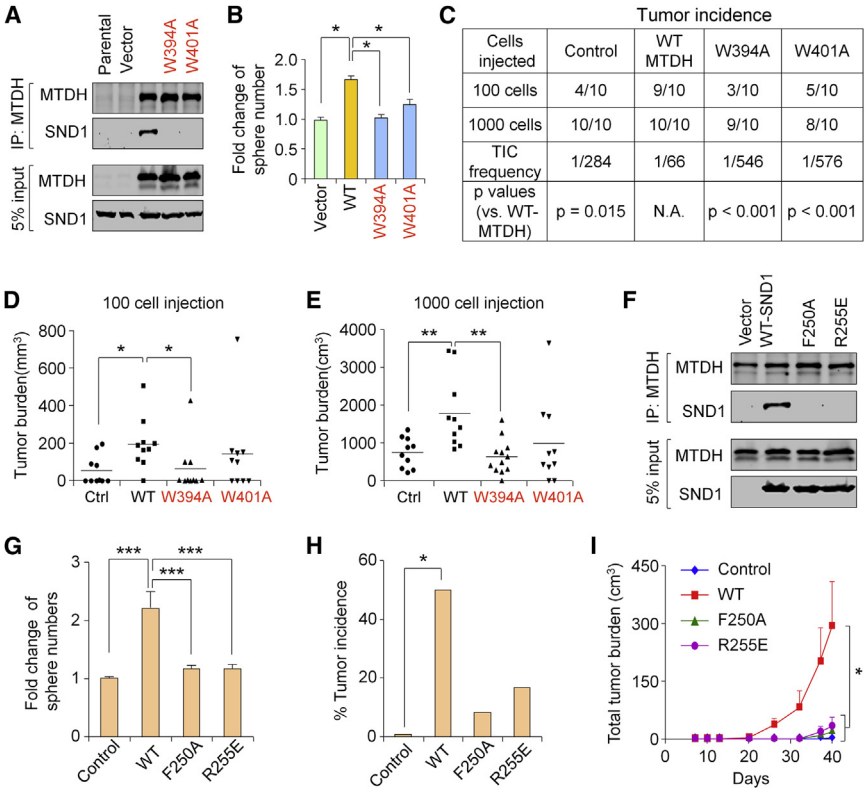

Cells injected	Control	WT MTDH	W394A	W401A
100 cells	4/10	9/10	3/10	5/10
1000 cells	10/10	10/10	9/10	8/10
TIC frequency	1/284	1/66	1/546	1/576
p values (vs. WT-MTDH)	p = 0.015	N.A.	p < 0.001	p < 0.001

Figure 4. Mutations in MTDH and SND1-Binding Residues Impair Tumor-Promoting Function

(A) Lysates from PyMT;*Mtdh*$^{-/-}$ tumor cells reconstituted with vector control, WT or mutant murine MTDH were immunoprecipitated with anti-MTDH antibody and immunoblotted for indicated proteins. Note all amino acid annotations are based on human MTDH. W394 and W401 of human MTDH correspond to W391 and W398 in murine MTDH, respectively.

(B) Mammosphere assays were performed with PyMT;*Mtdh*$^{-/-}$ tumor cells reconstituted with indicated MTDH constructs.

(C–E) In vivo tumor formation (C for tumor incidence; D and E for tumor volumes) was performed at limiting numbers using PyMT;*Mtdh*$^{-/-}$ tumor cells reconstituted with indicated WT or mutant MTDH.

(F) Lysates from SND1-KD PyMT;*Mtdh*$^{+/+}$ tumor cells reconstituted with vector control, WT, or mutant shRNA-resistant murine SND1 were immunoprecipitated with anti-MTDH antibody and immunoblotted for indicated proteins.

(G) Mammosphere assays were performed with SND1-KD PyMT;*Mtdh*$^{+/+}$ tumor cells reconstituted with vector control or indicated SND1 constructs.

(H and I) Mammary tumor incidence (H) and tumor growth curve (I) after orthotopic transplantations of SND1-KD PyMT;*Mtdh*$^{+/+}$ tumor cells reconstituted with indicated constructs.

Statistics: (B, G, and I) Student's t test. Data represent mean ± SEM. (C) Limiting dilution analysis. (D and E) Mann-Whitney test. (H) Chi-square test. ***p < 0.001, **p < 0.01, *p < 0.05. See also Figure S5.

mutations, including the negative control D389R, a mutation located outside the MTDH-SND1 interface, did not affect the interaction (Figure 3C). Likewise, the SND1 mutations that affected MTDH binding in vitro also affected the binding of full-length proteins in vivo to similar levels. Both WT HA-SND1 and the negative control mutant, HA-SND1 R316E, bound readily with Myc-MTDH, whereas other mutations, Δ39-43, F250A, or R255E, nearly completely abolished MTDH binding, and R324E significantly reduced the binding (Figure 3D).

The similar results of in vitro and in vivo studies of MTDH-SND1 interactions strongly suggest that the MTDH-SND1 interface characterized above dictates the interaction of the full-length MTDH and SND1 in mammalian cells. This allowed us to further define the role of this interface in controlling the function of MTDH and SND1 in cancer promotion.

MTDH Mutants Deficient in SND1 Binding Had Reduced Protumorigenic Activities

We recently demonstrated an essential role of MTDH in regulating mammary tumorigenesis (Wan et al., 2014). In particular, genetic deletion of *Mtdh* in mice impairs the tumor-initiating potential of mammary epithelial cells transformed by diverse oncogenes (PyMT, Wnt, ErbB2) or carcinogen stimuli, and this defect can be readily rescued by reintroducing MTDH into *Mtdh-knockout* (*Mtdh*$^{-/-}$) tumor cells by lentiviral transduction (Wan et al., 2014). To test whether interacting with SND1 is important for the tumor-initiating effect of MTDH, murine WT or mutant MTDH (W394A or W401A, corresponding mutations in mouse are W391A, W398A) was stably expressed in mammary tumor cells derived from *PyMT;Mtdh*$^{-/-}$ mice. The MTDH mutants W394A or W401A completely lost the ability to interact with SND1 (Figure 4A), suggesting that the SND1-interacting residues of MTDH are conserved between mouse and human. In vitro mammosphere formation assays showed that *PyMT;Mtdh*$^{-/-}$ tumor cells reconstituted with mutant MTDH formed a significantly lower number of spheres compared to those reconstituted with WT MTDH (Figure 4B). To examine how MTDH mutations affect tumor formation in vivo, we orthotopically transplanted *PyMT;Mtdh*$^{-/-}$ tumor cells into the mammary fat pads of WT recipient mice. We found that *PyMT;Mtdh*$^{-/-}$ tumor cells reconstituted with mutant MTDH contained substantially fewer tumor-initiating cells as revealed by reduced tumor incidence (Figure 4C) when a limited number of cells were injected. Furthermore, the size of tumors formed by *PyMT;Mtdh*$^{-/-}$ tumor cells reconstituted with mutant MTDH was much smaller than observed with WT MTDH (Figures 4D and 4E). Staining of Ki67 (Figure S5A) and cleaved caspase-3 (Figure S5B) was performed on these established tumors to examine their proliferation and apoptosis indices, respectively, and we did not observe significant differences across different groups. These results demonstrate that the interaction between MTDH and SND1 is essential for the protumorigenic activity of MTDH, and that this interaction

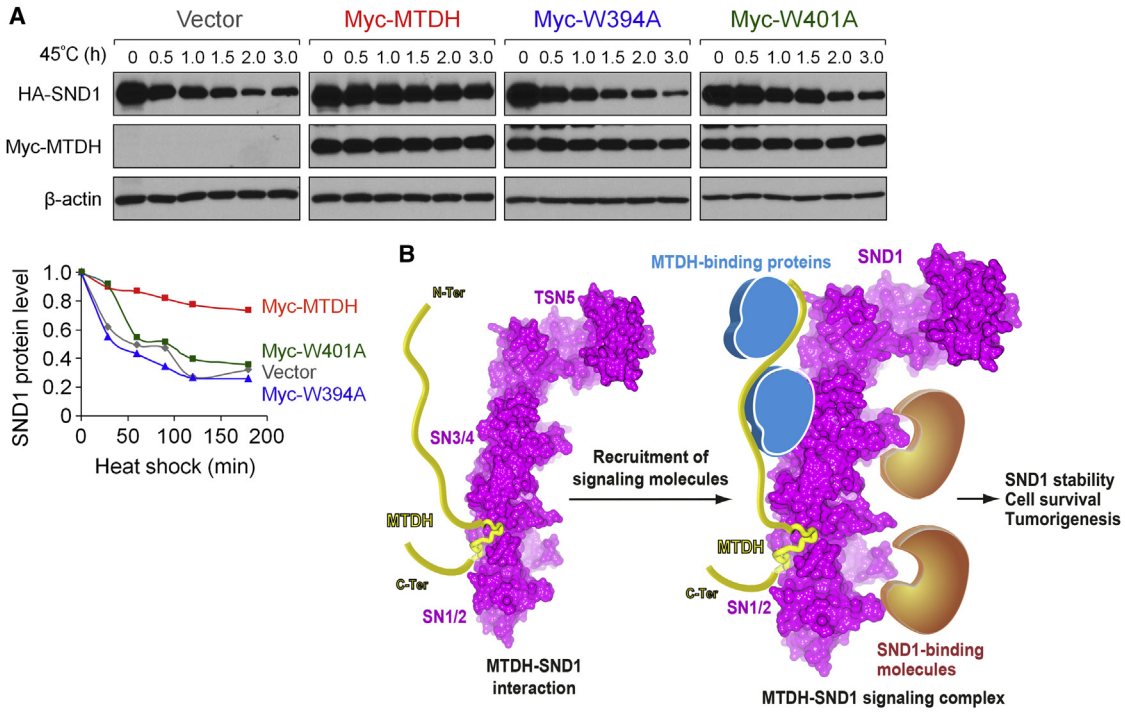

Figure 5. MTDH Interaction Protects SND1 from Heat Shock Stress-Induced Degradation

(A) HEK293T cells were transfected with HA-SND1 together with either empty vector control or indicated WT or mutant Myc-MTDH constructs. Two days postinfections, cells were treated under heat shock conditions, and lysates were immunoblotted for indicated proteins. β-actin was used as loading control. Representative results of three independent experiments are shown.

(B) The proposed mechanism of MTDH and SND1 in oncogenic signaling as a scaffold and a multidomain interacting protein, respectively, are illustrated using the structural model of the full-length MTDH-SND1 complex, modeled based on crystal structures of the MTDH (393–403)-SND1 (16–339) complex and the SN3/4-TSN5 domains of SND1 (PDB code: 3BDL).

contributes predominantly to tumor initiation, consistent with our recent findings (Wan et al., 2014).

SND1 Mutants Deficient in MTDH Binding Were Inactive in Tumor Promotion

The well-defined pockets in SND1 for MTDH binding and the role of this interaction in tumor initiation suggest that the protein pockets in SND1 represent a therapeutic target for cancer. We recently demonstrated that knockdown (KD) of SND1 impairs the tumor-initiating activities of *PyMT/Mtdh*$^{+/+}$ tumor cells, supporting a tumor-promoting role of SND1 (Wan et al., 2014). In the current study, a small hairpin RNA (shRNA)-resistant construct of WT or mutant SND1 (F250A or R255E) was stably expressed in SND1-KD *PyMT/Mtdh*$^{+/+}$ tumor cells, and their effects on tumor initiating activities were tested in vitro and in vivo. The SND1 mutations nearly completely abolished the MTDH interaction (Figure 4F). SND1 mutants barely increase the number of spheres formed in the in vitro mammosphere assays, whereas WT SND1 increases the sphere numbers by more than 2-fold compared to controls (Figure 4G). After transplantation of cells into mammary fat pads of recipient mice, WT SND1 markedly boosted tumor initiation and tumor growth as reflected by the increased tumor incidence and total tumor burden, whereas SND1 mutants exhibited very minor effects (Figures 4H and 4I). These results further support our conclusion that the interaction between MTDH and SND1 is important for tumor promotion, and that both MTDH-binding pockets in SND1 are crucial for this activity.

MTDH Mutants Deficient in SND1 Binding Failed to Stabilize SND1 under Stress

Our recent studies suggested that MTDH plays a key role in enhancing the stability of SND1 protein under stress conditions (Wan et al., 2014), which may contribute to the prosurvival role of SND1 in cancer cells under oncogenic or other stresses (Gao et al., 2010; Sundström et al., 2009; Weissbach and Scadden, 2012). To further substantiate this conclusion, we examined the effects of MTDH mutations on the cellular stability of SND1 during heat shock, a condition under which SND1 is important for cellular survival (Gao et al., 2010; Weissbach and Scadden, 2012). When overexpressed alone, the cellular level of HA-SND1 was rapidly reduced at 45°C, with a half-life of around 30 min (Figure 5A). Coexpression with WT Myc-MTDH augmented the cellular stability of HA-SND1 at 45°C, with the half-life extended beyond 3 hr, whereas coexpression of either MTDH mutants, W394A and W401A, failed to stabilize HA-SND1 during heat shock (Figure 5A). This result supports the role of MTDH-SND1 interaction in promoting the cellular stability of SND1, consistent with our recent observation that the protein levels of MTDH and SND1 are positively correlated in human breast cancers (Wan et al., 2014).

DISCUSSION

MTDH has gained increasing interest in recent years given its broad implication in diverse cancer types, and SND1 has been identified as a MTDH-binding protein that possesses tumor-promoting functions similar to MTDH (Emdad et al., 2013; Wan and Kang, 2013; Wan et al., 2014). However, the structural basis and functional significance of the MTDH-SND1 interaction remain unclear. The studies in this report mapped the minimal interaction motif/domain of MTDH and SND1 and determined the high-resolution crystal structure of their complex. Structural analysis and structure-guided functional studies showed that the MTDH-SND1 interface is essential for MTDH and SND1's activities in mammary tumor initiation and harbors structural features with promise as potential cancer therapeutic targets. In addition, the structure of the MTDH-SND1 complex provides an important platform for future understanding of cancer cell signaling bridged by this interaction.

The MTDH-SND1 interface characterized in this study provides key insights into the molecular basis of their interaction. The essential SND1-binding motif was previously mapped to two different regions of MTDH, residues 364–470 (Blanco et al., 2011) and 101–205 (Yoo et al., 2011). Our study here defined a short 11 residue peptide motif (residues 393–403) of MTDH as the primary SND1-binding motif, which is located within the fragment identified by Blanco et al. (2011). Mutations in either MTDH or SND1 at this interface abolish the interaction of the full-length proteins both in HEK293T cells and in breast tumor cells, supporting the notion that this interface is the dominant binding site between MTDH and SND1.

The prominent function of the MTDH-SND1 interface in cancer promotion suggests that targeting this interface might be a useful strategy for cancer therapy. In addition, our results suggest important ways for targeting this interface. The interaction between MTDH and SND1 is dominated by van der Waals contacts between W394 and W401 in MTDH and two well-defined hydrophobic pockets in SND1 that have the potential to bind small molecule inhibitors. Importantly, mutations in MTDH or SND1 at either binding pocket abolished their activity in promotion of mammary tumor initiation, thus making simultaneously targeting both SND1 pockets an attractive therapeutic approach. Other appealing features of this interface for targeting include the readily reversible binding between MTDH and SND1, suggesting that this interaction could be reversed by specific inhibitors. Furthermore, the MTDH-binding pockets are uniquely evolved in SN1/2 domains, but absent in other OB-fold superfamily proteins or other SN domains in SND1, underscoring the promise of developing highly specific compounds for blocking MTDH binding.

Such weak interactions are crucial for many important biological processes. For example, the weak interactions between protein phosphatase 2A (PP2A) and its phosphatase activator (PTPA) dictate a robust chaperone function of PTPA in PP2A activation (Guo et al., 2014). The transient recognition of herpesvirus-associated ubiquitin-specific protease (HAUSP) and its substrates p53 and MDM2 is crucial for deubiquitination of these important signaling proteins (Hu et al., 2006). Recognition of T cell receptors (TCRs) for peptides presented by major histocompatibility complex is also dictated by weak interactions (Birnbaum et al., 2014). Similar to our study here, the strategy of flexible fusion linkers to stabilize weak protein complexes had been utilized for crystallization of these complexes (Birnbaum et al., 2014; Guo et al., 2014; Hu et al., 2006). Recently, the structure of the AcrAB-TolC multidrug efflux pump was reported, where several flexible linkers were applied to stabilize the complex and facilitate crystallization (Du et al., 2014).

The structure of the MTDH-SND1 interface provides an important platform for understanding the cellular signaling coordinated by this interaction. Despite the structural similarity between SN1/2 and SN3/4 domains, SN3/4 does not possess the unique pockets and surface feature required for MTDH binding. The binding pocket for W401 harbors residues with multiple rotamers, where the van der Waals contact between W401A mutation and this pocket may be partially compensated by different side-chain conformations of these residues. In contrast, the binding pocket for W394 is formed by three proline residues, and its backbone structure could barely change the conformation to compensate for alteration at 394 of MTDH (Figure 2B, electrostatic potential). Furthermore, the hilly surfaces harboring protruding structures in SN1/2 and SN3/4 are distinctly different and are expected to confer different binding specificities. The domains in SND1 fragment containing SN3/4-TSN5 domains are arranged in a linear orientation with a crescent shape (Li et al., 2008) (Figure 5B). FRET analysis indicated that the distance between the termini of the full-length SND1 is farther than that of the SN3/4-TSN5 fragment (data not shown), suggesting that the multiple SND1 domains are arranged in a linear fashion (Figure 5B). This architecture likely allows different binding partners to be orchestrated in a coherent orientation for downstream signaling. Surprisingly, MTDH associates via a short peptide to a surface of SND1 that is rather flat and distinctly different from the hilly surface located on the opposite side of SND1. This simple mode of binding is in sharp contrast to the robust function of this interface in cancer promotion, suggesting that downstream signaling mediated by this interface might contribute to the multifaceted roles of MTDH and SND1 in cancer. Besides a single transmembrane domain, the entire 582 amino acid sequence of MTDH is largely disordered, suggesting the possibility that MTDH may interact with many signaling proteins. These features resemble signaling scaffold proteins, such as AKAPs (a kinase anchor protein; Gelman, 2012), suggesting that MTDH might function as a signaling scaffold protein. Together with SND1, MTDH might mediate cellular signaling via diverse signaling molecules orchestrated by the multiple interaction domains/motifs of SND1 and MTDH.

The reliance of SND1 stability on MTDH binding under stress provides another explanation for the role of MTDH-SND1 interaction in cancer. This result is also consistent with the observation that MTDH and SND1 are simultaneously elevated in tumor tissues (Wan et al., 2014; Wang et al., 2012). How the MTDH-SND1 interaction contributes to SND1 stability under stress, however, remains to be determined. Our in vitro study demonstrated that MTDH binding barely affects the thermal stability of SN1/2 domains or their sensitivity to protease cleavage (data not shown), suggesting that MTDH binding might not

directly stabilize SND1. Further studies are needed to decipher whether the cellular stability of SND1 relies on recruitment of other biomolecules.

EXPERIMENTAL PROCEDURES

Crystallization, Data Collection, and Structure Determination

Crystals of SND1 and MTDH fusion protein were grown at 20°C using the sitting-drop vapor-diffusion method by mixing 250 nl of 15 mg/ml SeMet-labeled SND1(16–339)-L21-MTDH (386–407) with 250 nl of well buffer (21.6% pEG3350, 0.1M sodium citrate [pH 8.0], 0.1M CsCl), plus 50 nl of micro seeds. Single crystals grew in 4 days and matured after 7 days. Crystals were gradually changed to well buffer with 0%–25% glycerol before being flash frozen in liquid nitrogen. A SAD data set useful for structure determination was collected and processed to 2.7 Å. X-ray diffraction data collection and structure determination are described in Supplemental Experimental Procedures. The final structure was refined to 2.7 Å (Table S1). Structural analysis, calculation of electrostatic potential, and structural presentation were performed using the program ccp4mg (McNicholas et al., 2011).

Tumorsphere and Tumorigenesis Assays

For tumorsphere analysis, single cells were plated in ultra-low attachment plates (Corning) with sphere media (1:1 DMEM: Ham's 12 supplemented with B27 (Invitrogen), 20 ng/ml EGF, 20 ng/ml basic fibroblast growth factor, and 4 μg/ml heparin). Spheres were counted 4–7 days after plating. For tumorigenesis assays, indicated numbers of PyMT tumor cells were transplanted into mammary fat of FVB recipient mice and tumor formations were monitored twice every week. Tumors were considered established when they became palpable for two consecutive weeks, and tumor size was measured by calipers for calculation of tumor volumes ($\pi \times \text{length} \times \text{width}^2/6$). All procedures involving mice and all experimental protocols were approved by Institutional Animal Care and Use Committee (IACUC) of Princeton University. Statistical analysis is described in Supplemental Experimental Procedures.

ACCESSION NUMBERS

The atomic coordinates of the MTDH-SND1 complex were deposited in the Protein Data Bank with accession code 4QMG.

SUPPLEMENTAL INFORMATION

Supplemental Information includes Supplemental Experimental Procedures, five figures, and one table and can be found with this article online at http://dx.doi.org/10.1016/j.celrep.2014.08.033.

AUTHOR CONTRIBUTIONS

F.G., V.S., and K.A.S. performed x-ray crystallographic analysis of the MTDH-SND1 complex. F.G., A.Z., and W.L. performed biochemical characterization of this interaction. L.W., Y.W., and M.S. analyzed the role of MTDH-SND1 interaction in breast cancer tumor models. Y.X. instructed the structural and biochemical studies, and Y.K. guided the tumor model studies. Y.X. wrote the manuscript, which was revised by L.W. and Y.K. and proofread by all authors.

ACKNOWLEDGMENTS

The use of Advanced Photon Source was supported by the U.S. Department of Energy under contract No. DE-AC02-06CH11357. LS-CAT Sector 21 was supported by the Michigan Economic Development Corporation and the Michigan Technology Tri-Corridor (grant 085P1000817). The work is supported by the NIH (R01GM69090 to Y.X. and R01CA134519 to Y.K.), ACS research scholar grant (118970 to Y.X.), Brewster Foundation (to Y.K.), Charlotte Elizabeth Procter Fellowship (L.W.), and the NIH National Center for Advancing Translational Sciences (NCATS), grant UL1TR000427.

Received: May 22, 2014
Revised: July 14, 2014
Accepted: August 15, 2014
Published: September 18, 2014

REFERENCES

Ash, S.C., Yang, D.Q., and Britt, D.E. (2008). LYRIC/AEG-1 overexpression modulates BCCIPalpha protein levels in prostate tumor cells. Biochem. Biophys. Res. Commun. *371*, 333–338.

Birnbaum, M.E., Mendoza, J.L., Sethi, D.K., Dong, S., Glanville, J., Dobbins, J., Ozkan, E., Davis, M.M., Wucherpfennig, K.W., and Garcia, K.C. (2014). Deconstructing the peptide-MHC specificity of T cell recognition. Cell *157*, 1073–1087.

Blanco, M.A., Alečković, M., Hua, Y., Li, T., Wei, Y., Xu, Z., Cristea, I.M., and Kang, Y. (2011). Identification of staphylococcal nuclease domain-containing 1 (SND1) as a Metadherin-interacting protein with metastasis-promoting functions. J. Biol. Chem. *286*, 19982–19992.

Callebaut, I., and Mornon, J.P. (1997). The human EBNA-2 coactivator p100: multidomain organization and relationship to the staphylococcal nuclease fold and to the tudor protein involved in Drosophila melanogaster development. Biochem. J. *321*, 125–132.

Caudy, A.A., Ketting, R.F., Hammond, S.M., Denli, A.M., Bathoorn, A.M., Tops, B.B., Silva, J.M., Myers, M.M., Hannon, G.J., and Plasterk, R.H. (2003). A micrococcal nuclease homologue in RNAi effector complexes. Nature *425*, 411–414.

Du, D., Wang, Z., James, N.R., Voss, J.E., Klimont, E., Ohene-Agyei, T., Venter, H., Chiu, W., and Luisi, B.F. (2014). Structure of the AcrAB-TolC multidrug efflux pump. Nature *509*, 512–515.

Emdad, L., Das, S.K., Dasgupta, S., Hu, B., Sarkar, D., and Fisher, P.B. (2013). AEG-1/MTDH/LYRIC: signaling pathways, downstream genes, interacting proteins, and regulation of tumor angiogenesis. Adv. Cancer Res. *120*, 75–111.

Gao, X., Ge, L., Shao, J., Su, C., Zhao, H., Saarikettu, J., Yao, X., Yao, Z., Silvennoinen, O., and Yang, J. (2010). Tudor-SN interacts with and co-localizes with G3BP in stress granules under stress conditions. FEBS Lett. *584*, 3525–3532.

Gelman, I.H. (2012). Suppression of tumor and metastasis progression through the scaffolding functions of SSeCKS/Gravin/AKAP12. Cancer Metastasis Rev. *31*, 493–500.

Guo, F., Stanevich, V., Wlodarchak, N., Sengupta, R., Jiang, L., Satyshur, K.A., and Xing, Y. (2014). Structural basis of PP2A activation by PTPA, an ATP-dependent activation chaperone. Cell Res. *24*, 190–203.

Hu, M., Gu, L., Li, M., Jeffrey, P.D., Gu, W., and Shi, Y. (2006). Structural basis of competitive recognition of p53 and MDM2 by HAUSP/USP7: implications for the regulation of the p53-MDM2 pathway. PLoS Biol. *4*, e27.

Lee, S.G., Kang, D.C., DeSalle, R., Sarkar, D., and Fisher, P.B. (2013). AEG-1/MTDH/LYRIC, the beginning: initial cloning, structure, expression profile, and regulation of expression. Adv. Cancer Res. *120*, 1–38.

Leverson, J.D., Koskinen, P.J., Orrico, F.C., Rainio, E.M., Jalkanen, K.J., Dash, A.B., Eisenman, R.N., and Ness, S.A. (1998). Pim-1 kinase and p100 cooperate to enhance c-Myb activity. Mol. Cell *2*, 417–425.

Li, C.L., Yang, W.Z., Chen, Y.P., and Yuan, H.S. (2008). Structural and functional insights into human Tudor-SN, a key component linking RNA interference and editing. Nucleic Acids Res. *36*, 3579–3589.

McNicholas, S., Potterton, E., Wilson, K.S., and Noble, M.E. (2011). Presenting your structures: the CCP4mg molecular-graphics software. Acta Crystallogr. D Biol. Crystallogr. *67*, 386–394.

Meng, X., Zhu, D., Yang, S., Wang, X., Xiong, Z., Zhang, Y., Brachova, P., and Leslie, K.K. (2012). Cytoplasmic Metadherin (MTDH) provides survival advantage under conditions of stress by acting as RNA-binding protein. J. Biol. Chem. *287*, 4485–4491.

Paukku, K., Yang, J., and Silvennoinen, O. (2003). Tudor and nuclease-like domains containing protein p100 function as coactivators for signal transducer and activator of transcription 5. Mol. Endocrinol. *17*, 1805–1814.

Ponting, C.P. (1997). P100, a transcriptional coactivator, is a human homologue of staphylococcal nuclease. Protein Sci. *6*, 459–463.

Sarkar, D., and Fisher, P.B. (2013). AEG-1/MTDH/LYRIC: clinical significance. Adv. Cancer Res. *120*, 39–74.

Sarkar, D., Park, E.S., Emdad, L., Lee, S.G., Su, Z.Z., and Fisher, P.B. (2008). Molecular basis of nuclear factor-kappaB activation by astrocyte elevated gene-1. Cancer Res. *68*, 1478–1484.

Scadden, A.D. (2005). The RISC subunit Tudor-SN binds to hyper-edited double-stranded RNA and promotes its cleavage. Nat. Struct. Mol. Biol. *12*, 489–496.

Shaw, N., Zhao, M., Cheng, C., Xu, H., Saarikettu, J., Li, Y., Da, Y., Yao, Z., Silvennoinen, O., Yang, J., et al. (2007). The multifunctional human p100 protein 'hooks' methylated ligands. Nat. Struct. Mol. Biol. *14*, 779–784.

Sundström, J.F., Vaculova, A., Smertenko, A.P., Savenkov, E.I., Golovko, A., Minina, E., Tiwari, B.S., Rodriguez-Nieto, S., Zamyatnin, A.A., Jr., Välineva, T., et al. (2009). Tudor staphylococcal nuclease is an evolutionarily conserved component of the programmed cell death degradome. Nat. Cell Biol. *11*, 1347–1354.

Theobald, D.L., Mitton-Fry, R.M., and Wuttke, D.S. (2003). Nucleic acid recognition by OB-fold proteins. Annu. Rev. Biophys. Biomol. Struct. *32*, 115–133.

Thirkettle, H.J., Mills, I.G., Whitaker, H.C., and Neal, D.E. (2009). Nuclear LYRIC/AEG-1 interacts with PLZF and relieves PLZF-mediated repression. Oncogene *28*, 3663–3670.

Tong, X., Drapkin, R., Yalamanchili, R., Mosialos, G., and Kieff, E. (1995). The Epstein-Barr virus nuclear protein 2 acidic domain forms a complex with a novel cellular coactivator that can interact with TFIIE. Mol. Cell. Biol. *15*, 4735–4744.

Välineva, T., Yang, J., Palovuori, R., and Silvennoinen, O. (2005). The transcriptional co-activator protein p100 recruits histone acetyltransferase activity to STAT6 and mediates interaction between the CREB-binding protein and STAT6. J. Biol. Chem. *280*, 14989–14996.

Välineva, T., Yang, J., and Silvennoinen, O. (2006). Characterization of RNA helicase A as component of STAT6-dependent enhanceosome. Nucleic Acids Res. *34*, 3938–3946.

Wan, L., and Kang, Y. (2013). Pleiotropic roles of AEG-1/MTDH/LYRIC in breast cancer. Adv. Cancer Res. *120*, 113–134.

Wan, L., Lu, X., Yuan, S., Wei, Y., Guo, F., Shen, M., Yuan, M., Chakrabarti, R., Hua, Y., Smith, H.A., et al. (2014). MTDH-SND1 Interaction Is Crucial for Expansion and Activity of Tumor-Initiating Cells in Diverse Oncogene- and Carcinogen-Induced Mammary Tumors. Cancer Cell *26*, 92–105.

Wang, N., Du, X., Zang, L., Song, N., Yang, T., Dong, R., Wu, T., He, X., and Lu, J. (2012). Prognostic impact of Metadherin-SND1 interaction in colon cancer. Mol. Biol. Rep. *39*, 10497–10504.

Weissbach, R., and Scadden, A.D. (2012). Tudor-SN and ADAR1 are components of cytoplasmic stress granules. RNA *18*, 462–471.

Yang, J., Aittomäki, S., Pesu, M., Carter, K., Saarinen, J., Kalkkinen, N., Kieff, E., and Silvennoinen, O. (2002). Identification of p100 as a coactivator for STAT6 that bridges STAT6 with RNA polymerase II. EMBO J. *21*, 4950–4958.

Yoo, B.K., Santhekadur, P.K., Gredler, R., Chen, D., Emdad, L., Bhutia, S., Pannell, L., Fisher, P.B., and Sarkar, D. (2011). Increased RNA-induced silencing complex (RISC) activity contributes to hepatocellular carcinoma. Hepatology *53*, 1538–1548.